



Delft University of Technology

## Performance analysis of an idealized Darrieus–Savonius combined vertical axis wind turbine

Pan, Jingna; Ferreira, Carlos; van Zuijlen, Alexander

### DOI

[10.1002/we.2904](https://doi.org/10.1002/we.2904)

### Publication date

2024

### Document Version

Final published version

### Published in

Wind Energy

### Citation (APA)

Pan, J., Ferreira, C., & van Zuijlen, A. (2024). Performance analysis of an idealized Darrieus–Savonius combined vertical axis wind turbine. *Wind Energy*. <https://doi.org/10.1002/we.2904>

### Important note

To cite this publication, please use the final published version (if applicable).  
Please check the document version above.

### Copyright

Other than for strictly personal use, it is not permitted to download, forward or distribute the text or part of it, without the consent of the author(s) and/or copyright holder(s), unless the work is under an open content license such as Creative Commons.

### Takedown policy

Please contact us and provide details if you believe this document breaches copyrights.  
We will remove access to the work immediately and investigate your claim.

## RESEARCH ARTICLE

WILEY

# Performance analysis of an idealized Darrieus–Savonius combined vertical axis wind turbine

Jingna Pan  | Carlos Ferreira | Alexander van Zuijlen

Faculty of Aerospace Engineering, Delft  
University of Technology, Delft, The  
Netherlands

**Correspondence**

Jingna Pan, Faculty of Aerospace Engineering,  
Delft University of Technology, Kluyverweg  
1, 2629 HS, Delft, The Netherlands.  
Email: [J.Pan-1@tudelft.nl](mailto:J.Pan-1@tudelft.nl)

**Funding information**

China Scholarship Council, Grant/Award  
Number: 201906450032

**Abstract**

To investigate the effect of force distributions of each turbine component on the power performance of the Darrieus–Savonius combined vertical axis wind turbine (hybrid VAWT), the hybrid VAWT is modeled as idealized turbine under various force distributions. The goal of idealization is to simplify the intricate interactions between the Savonius and Darrieus components. The simulation actuator surfaces with uniform force distributions lead to a cost-effective way to identify the optimal force distribution of each turbine component. The numerical model was validated against momentum theory. The results demonstrated that the numerical and theoretical results yield similar predictions in the low-thrust cases but show differences in the high-thrust cases. The maximum power coefficient  $c_{p_{max}}$  of an idealized hybrid VAWT with given thrust coefficient  $c_{T_{AD}}$  is lower than that of a single actuator. This is a consequence of the nonoptimal loading on the actuator. The results indicate that an idealized hybrid VAWT does not show a significant power increase compared with an optimal single Darrieus rotor. Therefore, the presence of a Savonius rotor inside a Darrieus rotor leads to a lower power output in any circumstance. The hybrid configuration is primarily advantageous for the start-up performance of the combined rotor, which is not explored in this study.

**KEYWORDS**

actuator-disk-in-cylinder model, Darrieus–Savonius combined vertical axis wind turbine (hybrid VAWT), power performance, uniform force distribution

## 1 | INTRODUCTION

Vertical axis wind turbines (VAWTs) have grown in popularity due to their multiple benefits in urban applications. Savonius and Darrieus rotors represent drag-type and lift-type VAWTs, respectively. They are compatible with omnidirectional installation and low-cost maintenance. A Savonius rotor is capable of self-starting at low wind speeds,<sup>1–3</sup> and the H-type Darrieus rotor can operate with the optimum tip speed ratio (TSR) range of 2.5–4.5, achieving a high power coefficient.<sup>4–7</sup> In contrast to the single Darrieus rotors, the Darrieus–Savonius combined vertical axis wind turbine (hybrid VAWT) was designed to possess high starting torque. A schematic of a two-dimensional (2D) hybrid VAWT is shown in Figure 1. Despite its good start-up performance, the power coefficient remains a significant concern for the hybrid VAWT. The hybrid VAWT can start up as efficiently as the single Savonius rotor but has a lower power coefficient than the single Darrieus rotor.<sup>8–10</sup> The benefits of the hybrid VAWT configuration have not been clarified yet.

This is an open access article under the terms of the [Creative Commons Attribution-NonCommercial-NoDerivs](https://creativecommons.org/licenses/by-nc-nd/4.0/) License, which permits use and distribution in any medium, provided the original work is properly cited, the use is non-commercial and no modifications or adaptations are made.

© 2024 The Authors. *Wind Energy* published by John Wiley & Sons Ltd.

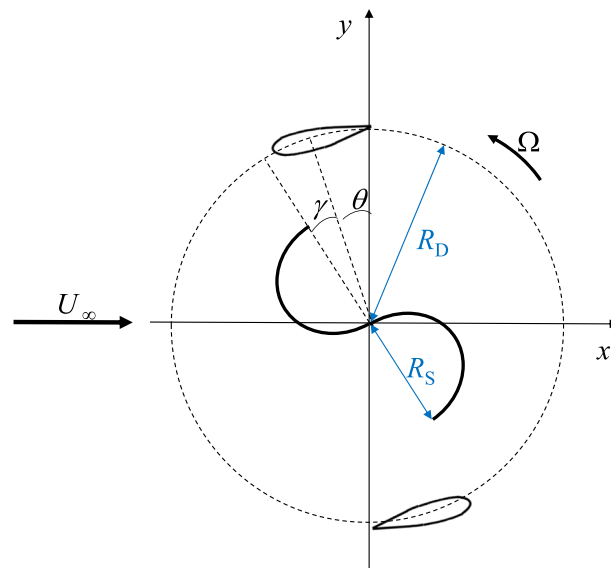


**FIGURE 1** Schematic of a hybrid VAWT with two semicircular Savonius blades and two Darrieus blades. VAWT, vertical axis wind turbine.

Researchers have been putting efforts into improving the performance of the hybrid VAWT. They mostly focused on optimizing the parameters, including but not limited to the installation position of the Savonius blade, radius ratio  $\frac{R_D}{R_S}$ , and attachment angle  $\gamma$ . Sun et al.<sup>8</sup> investigated the effect of Savonius blade's installation position and observed that the power coefficient of the hybrid VAWT was lower than the single Darrieus rotor. In accordance with the rationale of Sun et al.,<sup>8</sup> the poor power performance of the hybrid VAWT was due to the low pressure difference on the Darrieus blade of the hybrid VAWT compared with that of the stand-alone Darrieus rotor at most angular positions. Pallotta et al.<sup>9</sup> conducted a series of PIV experiments on a hybrid VAWT. Their measurements revealed a reduction of approximately 20% in the power coefficient compared with a stand-alone Darrieus turbine. However, it is unknown whether the optimization of Darrieus blades and/or Savonius blades would contribute to the power increase of the hybrid VAWT compared with a single Darrieus. To gain further insights into the hybrid VAWT, this paper investigates the extent to which the power coefficient of the idealized hybrid VAWT can be increased by excluding geometrical and operational effects (airfoil shape, rotor shape, installation position of each component and TSR of a real hybrid VAWT). This paper aims to determine the maximum power that can be extracted by the idealized hybrid VAWT and identify its optimal operating conditions.

The modeling of the hybrid VAWT plays an important role in predicting the turbine performance and developing stages such as design, construction, and operation. In recent years, many studies have been conducted in developing numerical models for hybrid VAWT. Chegini et al.<sup>11</sup> investigated the self-starting performance of a hybrid VAWT and techniques of power performance enhancement (deflectors). A 2D computational fluid dynamics (CFD) approach was used to simulate the hybrid VAWT. The complex flow around the turbine and transient blade forces were obtained by solving the unsteady Reynolds-averaged Navier–Stokes (URANS) equations. Pouransari et al.<sup>12</sup> examined the performance of three hybrid VAWTs using a numerical approach to solve the three-dimensional (3D) URANS equations. Their study revealed that a hybrid VAWT with the Savonius above the Darrieus can generate more power than a conventional hybrid VAWT. Irawan et al.<sup>13</sup> studied the improvements of the hybrid VAWT using the CFD approach. The 2D URANS equations were solved to obtain the complex flow problems in Ansys Fluent. The results showed that power coefficients can be achieved up to 50% higher by changing the turbine rotation mode compared with the conventional hybrid VAWT.

The complexity of these numerical models increases with the need to acquire knowledge of blade-vortex interactions and blade forces. In principle, most of these numerical models are based on the real geometry of the turbine blade. However, it is obvious that the blade rotation can be interpreted as forces acting on the flow, and the turbine power is determined by the force distribution along the rotation path in Figure 1. The flow models of the hybrid VAWT remain a challenge. The motivation of this paper is to extend the knowledge of wind energy conversion in a hybrid VAWT flow model.

This study aims to explore the optimal power performance of a hybrid VAWT using flow models. Wind turbine flow models can be classified into kinematic models and dynamic models according to the boundary conditions.<sup>14</sup> The vortex model is popular in the group of kinematic models. It solves the potential flow problem using the Neumann boundary condition on the impermeable surface. Besides, the time rate of circulation change in a control volume is conserved as zero. Ferreira<sup>15</sup> conducted 2D and 3D potential flow simulations to gain insights into the aerodynamics of VAWT. Jin et al.<sup>16</sup> investigated 2D unsteady flows around polygons using a vortex method. Pan et al.<sup>17</sup> implemented the vortex particle method to simulate transient blade forces and wake fields around the turbine. The kinematic models are quite complex due to the necessity of solving the unsteadiness of flow.

The dynamics models have been widely used due to their simplicity. They are based on momentum conservation. Mohammed et al<sup>18</sup> provided a review of various momentum models used in the aerodynamic modeling of Darrieus rotors. It discusses three streamtube models as follows: single streamtube (SST), multiple streamtube (MST), and double multiple streamtube (DMST). The former two models have the same problem that a constant velocity along the streamtube is assumed. DMST overcomes this problem by accounting for the velocity variation along the streamtube. However, it has a convergence issue at high TSRs. Froude<sup>19</sup> originally proposed an actuator disk model for horizontal axis wind turbines (HAWTs). This simplified model is commonly employed for propellers or HAWTs, representing a permeable surface with uniformly distributed forces. The flow induced by this force distribution is characterized by shedding vorticity. In the case of VAWTs, where the blade path follows a circular trajectory, the information available is limited to the streamwise direction using the actuator disk model. Madsen<sup>20</sup> proposed an alternative actuator cylinder model for VAWTs, distributing forces along a cylindrical surface. Both actuator models are created based on the blade forces acting on the fluid. However, the diffusivity is not included in these models.

In the current study, a 2D idealized hybrid VAWT, comprising a Darrieus part and a Savonius part, is investigated. To estimate the power performance of the hybrid VAWT while excluding kinematic and structural effects, an idealized hybrid VAWT is implemented in OpenFOAM as momentum sources. The Darrieus part is represented by a uniformly loaded actuator cylinder, while the Savonius part is represented by a uniformly loaded actuator disk. This approach allows us to examine the power gain or loss of the hybrid VAWT in an ideal simulation, considering variations in the location and force distribution on the actuators. It is worth noting that the maximum power coefficient  $c_{p_{ideal}}$  of 0.616 can be achieved with uniform force distributions along the actuator cylinder.<sup>21</sup> This value exceeds the maximum  $c_p$  of the actuator disk. Our study primarily relies on numerical simulations to investigate the effect of force distribution on power output of the idealized hybrid VAWT. Section 2 describes the theoretical and numerical models of the actuator disk and actuator cylinder. In Section 3, different force distributions of hybrid turbines are investigated based on the extracted power and velocity fields. Finally, Section 4 summarizes our findings.

## 2 | METHODOLOGY

This section discusses the similarities and differences between theoretical and numerical actuator models. An idealized hybrid VAWT in the numerical model is represented by two actuator surfaces: a circular surface for the Darrieus part and a thin rectangular surface for the Savonius part. The blade forces act on the flow as distributed body forces along the actuator surfaces. First, the relation between vorticity and force is derived. The theoretical models of the actuator disk and actuator cylinder are also presented.

Subsequently, the OpenFOAM model simulating the idealized hybrid VAWT with uniform loading is proposed.

### 2.1 | Simplification of vorticity evolution

Given the assumption of a 2D incompressible and inviscid flow around the idealized hybrid VAWT, the vorticity equation is expressed as Equation (1) without vorticity turning, stretching, and diffusion. The term  $\frac{D\vec{\omega}}{Dt}$  on the left-hand side denotes the material derivative of the vorticity vector  $\vec{\omega}$ . It is the rate of change of vorticity of the moving fluid particle. This equation indicates that vorticity can only be introduced by a change of external body forces  $\vec{f}$ . The force distribution of a 2D actuator with uniform loading is represented by Equation (2), where  $f_x$  and  $f_y$  denote body forces in the  $x$  and  $y$  directions. In the case of actuator disk,  $f_y$  is equal to zero.

$$\frac{D\vec{\omega}}{Dt} = \nabla \times \vec{f} \quad (1)$$

$$\vec{f} = [f_x \ f_y \ 0]^T \quad (2)$$

Substitution of Equation (2) into Equation (1) leads to the following:

$$\frac{D\vec{\omega}}{Dt} = \begin{bmatrix} 0 \\ 0 \\ \frac{\partial f_y}{\partial x} - \frac{\partial f_x}{\partial y} \end{bmatrix} \quad (3)$$

Hence, the shedding vorticity only appears when  $\frac{\partial f_y}{\partial x} - \frac{\partial f_x}{\partial y}$  is nonzero. As the actuator models characterize the flow as vortices by the change of the force distribution, the vorticity fields of the theoretical actuator disk and actuator cylinder models will be investigated in Section 3.1. The

force discontinuity is used to represent the hybrid VAWT model in this study. This assumption potentially ignores the effect of blade shape on the performance of the hybrid VAWT.

## 2.2 | Theoretical actuator model

A brief introduction of the existing theoretical actuator models is presented, emphasizing the specific implementations used in this study. Extensive references are suggested for more detailed information about the overview of the actuator disk model<sup>19</sup> and actuator cylinder model.<sup>20</sup> This work investigates the case of an idealized turbine with uniform force distribution, where the viscosity is neglected. The heat transfer is also not included in this study. So, the flow problem is simplified as a 2D steady inviscid incompressible flow with constant internal energy.

The actuator disk model is illustrated in Figure 2A. In this model, the flow problem is assumed to be solved along the axial axis. The relation between the velocity at the disk  $U_R$  and the freestream upwind velocity  $U_\infty$  is expressed through an induction factor  $a$ , shown in Equation (4). The induction factor  $a$  is obtained by equating expressions of streamtube dynamics, representing the change in wind speed normalized by  $U_\infty$ .

$$U_R = U_\infty(1 - a) \quad (4)$$

The thrust and power coefficients are calculated as  $c_T = 4a(1 - a)$  and  $c_p = 4a(1 - a)^2$  according to the momentum theory. The relation of power coefficient  $c_p$  and thrust coefficient  $c_T$  is theoretically expressed as  $c_p = c_T(0.5 + 0.5\sqrt{1 - c_T})$ . The maximum power that can be extracted by a wind turbine is known as the Betz limit and corresponds to  $c_{p\text{Betz}} = 16/27$ ,  $c_{T\text{Betz}} = 8/9$  and  $a = 1/3$ .<sup>22</sup>

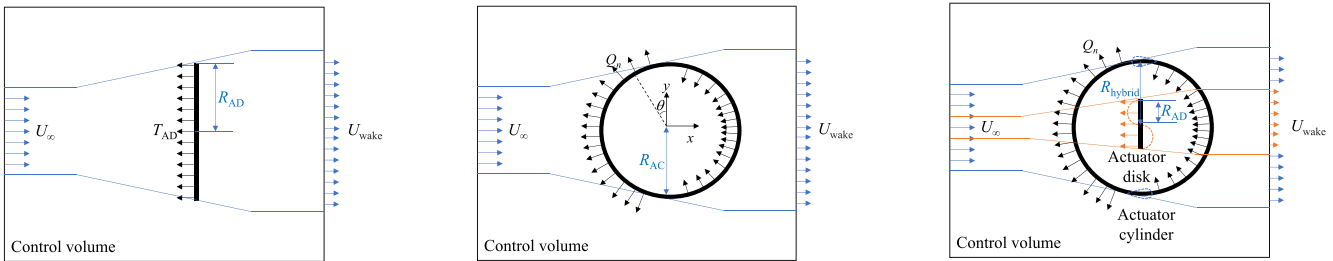
The actuator cylinder model is a 2D dynamic model extending the application of the actuator disk model, except that the actuator cylinder model is used in two directions rather than only one axial direction. A schematic of the actuator cylinder for VAWT is shown in Figure 2B, where the body forces in the normal direction are denoted as  $Q_n$ .

Given the same thrust coefficient, the distribution of the volumetric force along the actuator is implemented differently for the two models. For the actuator disk, the volumetric force is evenly added to each cell of the actuator in the  $x$  direction according to the given thrust. In the case of the actuator cylinder, the force components in the normal direction  $Q_n$  are evenly distributed along the actuator. It is calculated from

$$Q_n = \frac{T}{\sum_{i=0}^n (\vec{e}_{n_i} \cdot \vec{e}_{x_i})}, \text{ where } \vec{e}_{n_i} \text{ and } \vec{e}_{x_i} \text{ are the unit vectors in the normal and } x\text{-axis directions, respectively. The denominator } \sum_{i=0}^n (\vec{e}_{n_i} \cdot \vec{e}_{x_i}) \text{ is the sum}$$

of the normal vectors' projection on the  $x$ -axis, and  $n$  is the number of cells that fall into the actuator region. The current work focuses on a 2D idealized hybrid VAWT, which can be represented by placing an actuator disk inside an actuator cylinder. The schematic of the idealized hybrid VAWT is depicted in Figure 2C. It is worth noting that the  $c_{T_{AD}}$ ,  $c_{T_{AC}}$ , and  $c_{T_{\text{hybrid}}}$  represent thrust coefficients of the AD, AC, and idealized hybrid VAWT, which are nondimensionalized by their respective radii ( $R_{AD}$ ,  $R_{AC}$ ,  $R_{\text{hybrid}} = R_{AC}$ ). The thrust coefficient of the idealized hybrid VAWT corresponds to the outer radius, given by  $c_{T_{\text{hybrid}}} = c_{T_{AC}} + c_{T_{AD}} \cdot \frac{R_{AD}}{R_{AC}}$ .

Given the uniform force distribution along different actuator surfaces, the vorticity shedding depends on the gradient of body forces according to the vorticity equation in Section 2.1. So, the idealized hybrid VAWT in Figure 2C can be superimposed to one single actuator as shown in Figure 3. The force distribution becomes nonuniform with the superimposed force  $T_{AD}$  in the center and the original force  $T_{AC}$ .



(A) Actuator disk

(B) Actuator cylinder

(C) Idealized hybrid VAWT

**FIGURE 2** (A–C) Schematic of actuator models for the idealized turbine.

## 2.3 | Numerical actuator model

### 2.3.1 | Set-up

The force distribution is prescribed as uniform along the disk or cylinder with a thickness of 3.38% of the cylinder's dimension. This ensures that the actuator cylinder is aligned with the cylindrical mesh shown in Figure 4B. In this work, the 2D flow fields of the actuator disk, actuator cylinder, and idealized hybrid VAWT are simulated in OpenFOAM 4.1.<sup>23</sup> The steady laminar solver simpleFoam is employed with a Reynolds number of  $9.67e5$ . The computational domain and mesh are shown in Figure 4. The domain size is  $50R_{AC}$  in the x-direction and  $30R_{AC}$  in the y-direction. The numerical power output for cell  $i$  can be obtained from  $\vec{F}_i \cdot V_i \cdot \vec{u}_i$ , where  $\vec{F}_i$  is volume force with a unit of  $N/m^3$ ,  $V_i$  is the volume of cell  $i$ , and  $\vec{u}_i$  is the local velocity at cells where forces are exerted.

Mesh independence for the single AC ( $c_{T_{AC}} = 0.93$ ) and hybrid VAWT with upwind AD ( $c_{T_{AC}} = 0.89$ ,  $c_{T_{AD}} = 0.09$ ) is shown in Table 1. The power coefficient is obtained from simulations with different cell numbers. Three configurations for actuator thickness are studied for the single AC with  $c_{T_{AC}} = 0.85$ . The thickness of  $3.38\%D_{AC}$ ,  $5.07\%D_{AC}$ , and  $6.76\%D_{AC}$  is applied to the AC with body force exerted into three, four, and six

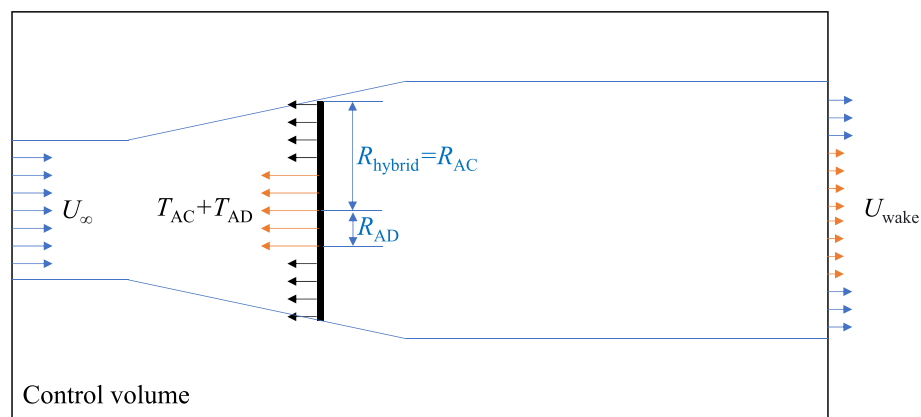


**FIGURE 3** Schematic of actuator disk model with nonuniform force distribution.

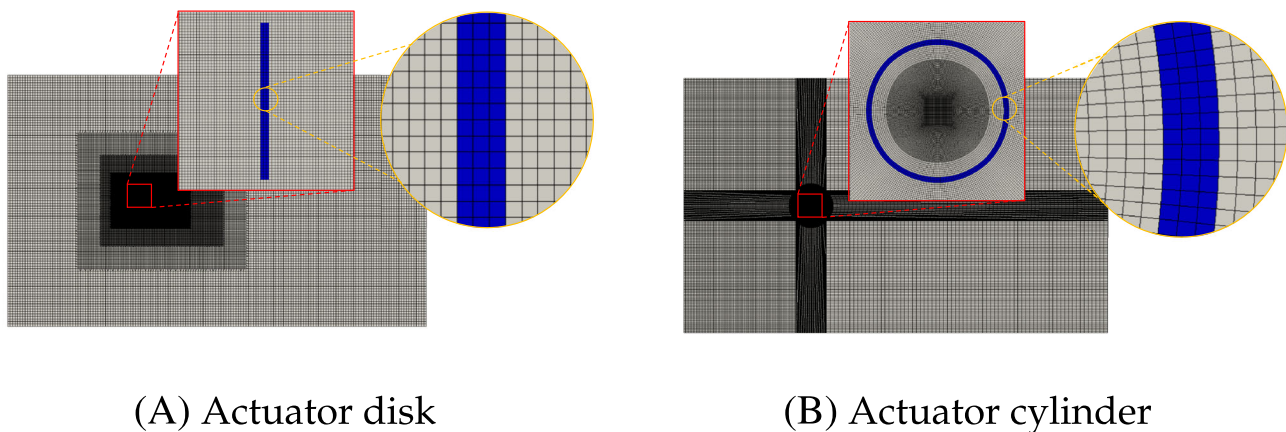


**FIGURE 4** (A, B) Computational domain and mesh in OpenFOAM simulations.

**TABLE 1** Mesh independence for power coefficient of AC and idealized hybrid VAWT with upwind AD.

Cell number	7.6e4	8.1e4	8.8e4	1.0e5	1.8e5
AC	0.59544 (+0.48%)	0.59581 (+0.54%)	0.59614 (+0.60%)	0.59545 (+0.48%)	0.59559 (+0.51%)
Hybrid VAWT	0.57740	0.57670	0.57694	0.57603	0.57563

Abbreviations: AC, actuator cylinder; AD, actuator disk; VAWT, vertical axis wind turbine.

layers of cells, respectively. The purpose of this analysis is to determine the mesh configuration and actuator thickness required for accurate results while considering the computational cost. The power coefficient  $c_p$  obtained from the three configurations of thickness is predicted as 0.58530, 0.63049, and 0.65858, with discrepancies of  $-0.73\%$ ,  $+6.93\%$ , and  $+11.70\%$  compared with the theoretical results. So, the thickness of  $3.38\%D_{AC}$  with three layers for AC yields a better prediction than the other two thickness configurations. The five mesh configurations predict discrepancies of  $+0.48\%$ ,  $+0.54\%$ ,  $+0.60\%$ ,  $+0.48\%$ , and  $+0.51\%$  compared with  $c_{p_{Betz}}$ . It is observed that a cell number of  $8.8e4$  is chosen to balance computational cost and accuracy for both the single actuator and hybrid actuator cases. Compared with the refined mesh cases, the numerical discrepancies are found to be 0.092% for the single actuator simulation and 0.23% for the hybrid actuator simulation. These errors indicate the deviation of the results obtained with the chosen cell number from the more refined solutions.

### 2.3.2 | Differences between theoretical and numerical methods

In OpenFOAM, the Navier–Stokes (NS) equation<sup>24</sup> for incompressible flow considering the force field of the actuator is shown in Equation (5), where the diffusion term is included. However, the theoretical methods ignore this term.

$$\frac{\partial \vec{u}}{\partial t} + (\vec{u} \cdot \nabla) \vec{u} = -\frac{\nabla p}{\rho} + \nu \nabla^2 \vec{u} + \frac{\vec{F}}{\rho} \quad (5)$$

There are additional differences that need to be accounted for when comparing the theoretical actuator models to the numerical simulations:

- Thickness of the actuator surface: In theoretical actuator models, the actuator surface is assumed to have zero thickness. However, in numerical simulations using OpenFOAM, the actuator surface is represented by a finite thickness. This means that the body force applied to the flow should be distributed over the cell volumes in the computational domain rather than being concentrated on an infinitesimally thin surface.
- Force distribution at the tip: The theoretical actuator models may assume a discontinuity in the force distribution at the tip of the actuator surface. However, in numerical simulations, due to the finite thickness of the actuator surface, the point where the force discontinuity occurs may not align exactly with the theoretical location. The numerical method may introduce some deviations in the force distribution near the actuator tip.

## 3 | RESULTS AND DISCUSSIONS

### 3.1 | Comparison of stand-alone actuator models

The vorticity equation shown in Section 2.1 demonstrates that the shedding vorticity is characterized by force changes. To validate our numerical model, the actuator cylinder is categorized into three types of surface: circular surface, upwind-half circular surface, and downwind-half circular surface. The uniform force distributions of different actuators are depicted in Figure 5. The thrust coefficient  $c_T = 0.93$  is applied for the four actuators. The total thrust of the rotor  $T$  needs to be calculated and distributed along the actuator to implement the actuator disk and actuator cylinder model in OpenFOAM.

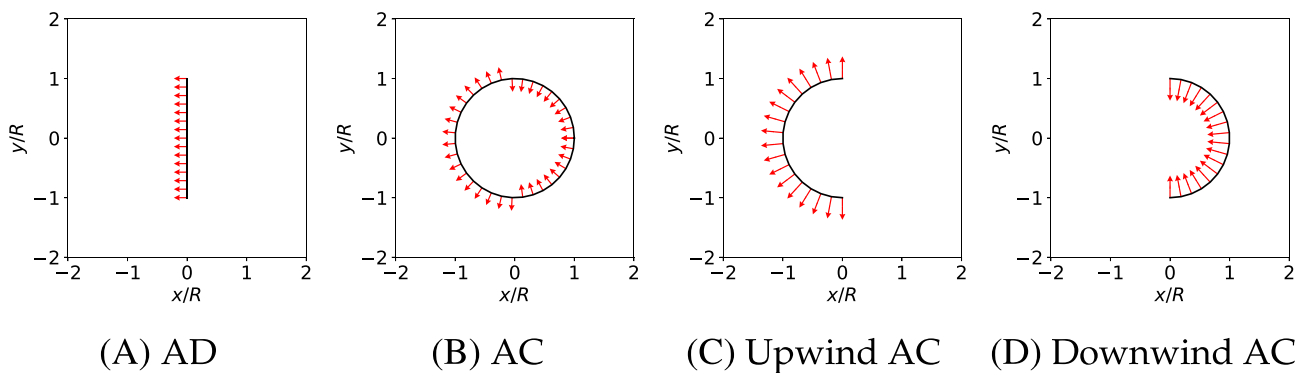


**FIGURE 5** (A–D) Force distribution of different actuators (red arrows represent vectors of body force).



The corresponding vorticity fields are shown in Figure 6. The vorticity originates from the top and bottom ends of an actuator, where the force discontinuity occurs. The expanded vorticity shedding is observed in four actuators. The similar vorticity distributions among the actuators indicate comparable flow mechanisms, emphasizing the role of force distribution changes in introducing vorticity described in Section 2.1. The power coefficients obtained from AD, AC, upwind AC, and downwind AC are 0.59115, 0.59614, 0.59566, and 0.59598, respectively. The visualizations of the four configurations provide valuable insights into flow patterns and contribute to optimizing the design and performance of the idealized hybrid VAWT.

The nondimensional flow velocity at the center of an actuator ( $x=0$ ) is depicted in Figure 7. The streamwise velocity shows a gradual decrease instead of a sudden drop at  $y/R = \pm 1$ .

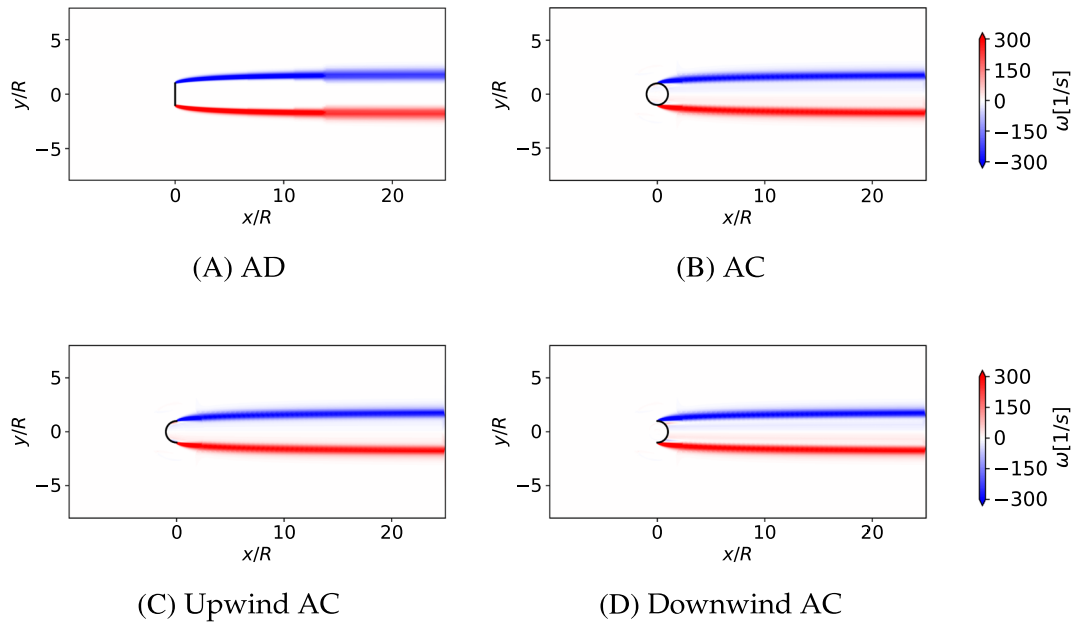


**FIGURE 6** (A–D) Vorticity fields of different actuators.

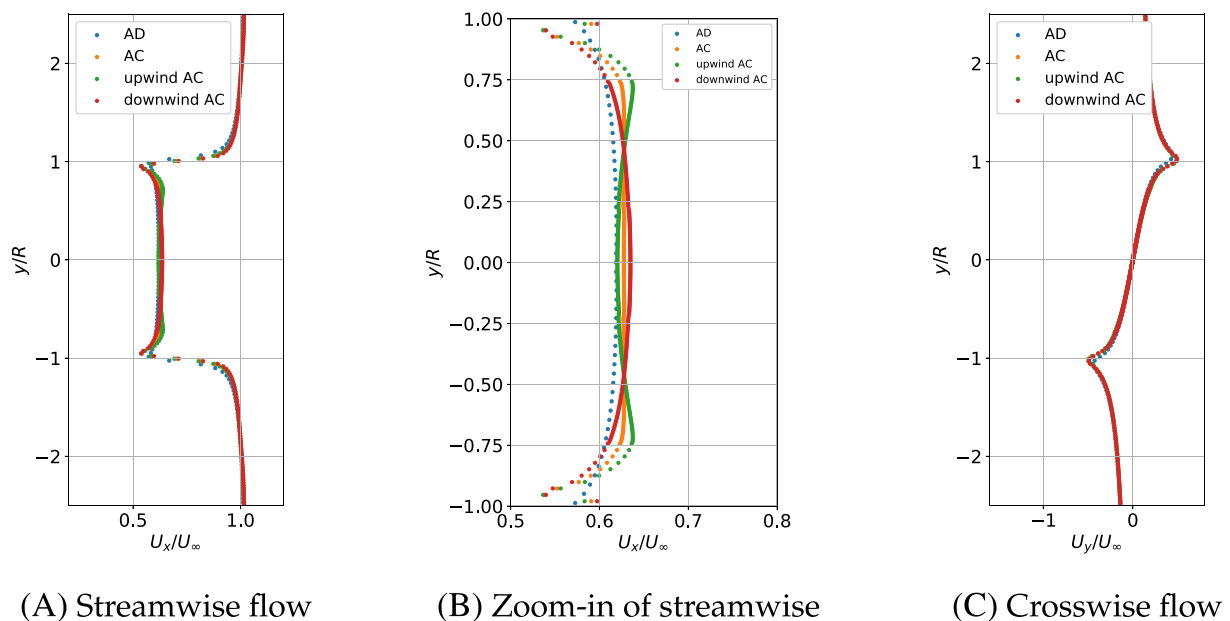


**FIGURE 7** (A–C) Nondimensional flow velocity at  $x=0$ .



The sampled flow velocity variations at the center of the four actuators have a similar trend in each direction (streamwise and crosswise directions) with negligible differences. The magnitude of minimum  $U_{x,x=0}$  for the AD case is around 5.97% higher than the other three AC cases. And the magnitude of minimum and maximum  $U_{y,x=0}$  for the AD case exhibits around 9.90% of differences compared with those for the other three AC cases. These negligible differences are attributed to the effect of volume force exerted into a finite thickness of cells in Figure 4. The above quantitative and qualitative comparisons demonstrate that the proposed numerical models can predict identical vorticity systems with the same thrust coefficient for the uniformly loaded actuator.

The nondimensional streamwise velocity and pressure distribution along the  $x$ -axis are depicted in Figure 8. It is observed that the pressure decreases at  $x/R=0$  for AD,  $x/R=\pm 1$  for AC,  $x/R=-1$  for upwind AC, and  $x/R=1$  for downwind AC. The streamwise velocity gradually decreases along the  $x$ -axis for the four actuators. The pressure reductions for the four actuators have the same amplitudes. The modeling of pressure drop occurs at the position where the body forces are exerted, yielding an effective numerical method.

The numerical model is further verified against the theoretical model in a range of thrust coefficients (0.171 to 1.026). A series of thrust coefficients are chosen to capture the trend of the power coefficient variation. Comparison between theoretical and numerical results of the variation of power coefficient  $c_p$  for an actuator cylinder with different thrust coefficients  $c_T$  is shown in Figure 9. It is observed that the numerical and theoretical results yield similar trends with  $c_T = 0.0$ –0.5. Between  $c_T = 0.5$  and 0.89, the numerical  $c_p$  is lower than the theoretical prediction. For  $c_T > 0.89$ , OpenFOAM tends to overestimate the  $c_p$ . The maximum power coefficient  $c_{p_{max}}$  is about 0.598% higher than the theoretical  $c_{p_{max}}$ . This difference is negligible, and it is expected due to the wake expansion (Figure 6) and the gradual velocity decrease at  $y/R = \pm 1$  (Figure 7) predicted by the numerical model. The validity of this assumption has also been demonstrated by De Tavernier.<sup>25</sup> The vorticity fields, velocity, and pressure

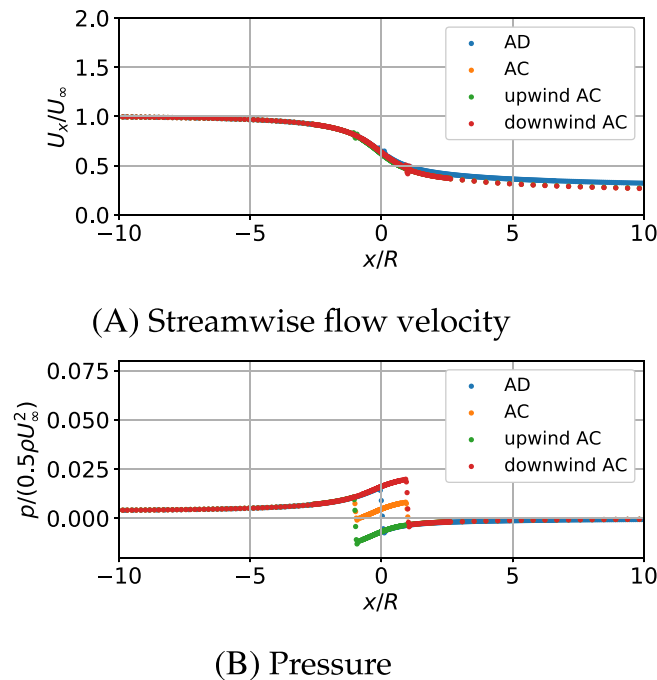


**FIGURE 8** (A, B) Nondimensional streamwise velocity and pressure distribution at  $y = 0$ .

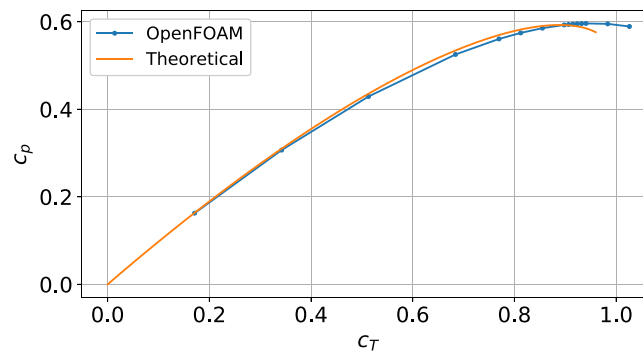


**FIGURE 9** Variation of power coefficient for AC with different  $c_T$  in theoretical and numerical solution. AC, actuator cylinder.

variations of the four actuators are identical with equivalent body force distributions. This equivalence demonstrates the validity of the proposed numerical model.

### 3.2 | Effect of force distribution on power performance of hybrid VAWT

#### 3.2.1 | Varied position of idealized Savonius, representing AD

To estimate the power of an idealized hybrid VAWT, the inner Savonius is represented by a uniformly loaded actuator disk, while the Darrieus rotor is idealized as a uniformly loaded actuator cylinder. The vorticity shedding depends on the force variation of the actuator. So, force distribution is the most relevant factor that affects the power performance of hybrid VAWT. Researchers have been putting efforts into implementing active pitch control to control blade forces so that a better power production is achieved from VAWTs. Bouzaher et al.<sup>26</sup> proposed a dynamic control device (a couple of flapping wings) for VAWT blades to get the optimum power harvesting. The control scheme reduces the negative effects of blade-vortex interaction on power production. They attempted to resolve the correlation between force distribution and power performance for the hybrid VAWT. Their study revealed that the total power of the hybrid VAWT varies with different rotor configurations. It indicates that the interaction between each component of hybrid VAWT is the main cause of power change. So, the position of the inner Savonius is varied to explore the optimal force distribution of the hybrid VAWT.

In this section, the impact of the inner AD's position in an idealized hybrid VAWT is investigated. By varying the position of the inner AD, we aim to understand its influence on the overall performance of the idealized hybrid VAWT. Given the assumption of two actuators mounted on the same rotational axis, the radius ratio of the outer and inner actuators is set as five.

It is known that the power output of the realistic hybrid VAWT is affected by the presence of inner Savonius. The power reduction of a Darrieus blade occurs mainly at the upwind and downwind region.<sup>27</sup> To understand the power generation mechanism of the hybrid VAWT, the upwind and downwind of the hybrid VAWT could be the most related region.

The inner AD acting as a turbine- or a propeller-mode is placed upwind, center, or downwind of the cylinder generating six kinds of force distributions. The force distributions for an idealized hybrid VAWT are depicted in Figures 10 and 11 with the same AC forces and different AD forces. The force directions of the inner AD are the same with the direction of x-axis in the turbine-mode case and opposite to the direction of x-axis in the propeller-mode case.

As the maximum power coefficient of the actuator disk theory is achieved when  $c_T = 0.89$ , the thrust coefficient for the outer actuator of the idealized hybrid VAWT is fixed as 0.89. The thrust coefficient for the inner actuator varies to investigate its impact on the overall power performance. Power coefficient of the aforementioned idealized hybrid VAWTs with varied  $c_{TAD}$  and  $c_{TAC} = 0.89$  is depicted in Figure 12. The x-axis is the thrust coefficient of the idealized hybrid VAWT  $c_{T_{hybrid}}$ , and the y-axis is the power coefficient of the idealized hybrid VAWT  $c_{p_{hybrid}}/c_{p_{Betz}}$  normalized by the optimal theoretical power coefficient of the single AC  $c_{p_{Betz}}$ . The results indicate that the power coefficient of idealized hybrid VAWT barely exceeds  $c_{p_{Betz}}$ , except when the low-thrust AD operates in a propeller mode. The idealized hybrid VAWT with a center turbine-mode AD has a higher power coefficient compared with idealized hybrid VAWT with upwind and downwind turbine-mode ADs. The maximum power extracted from idealized hybrid VAWT with upwind AD and given  $c_{TAC} = 0.89$  is around 0.435% higher compared with  $c_{p_{Betz}}$ . The negligible difference can be attributed to the modeling difference between the theoretical and numerical methods (Section 2.3.2). The hybrid VAWT cannot show a significant power increase compared with an optimal single Darrieus.

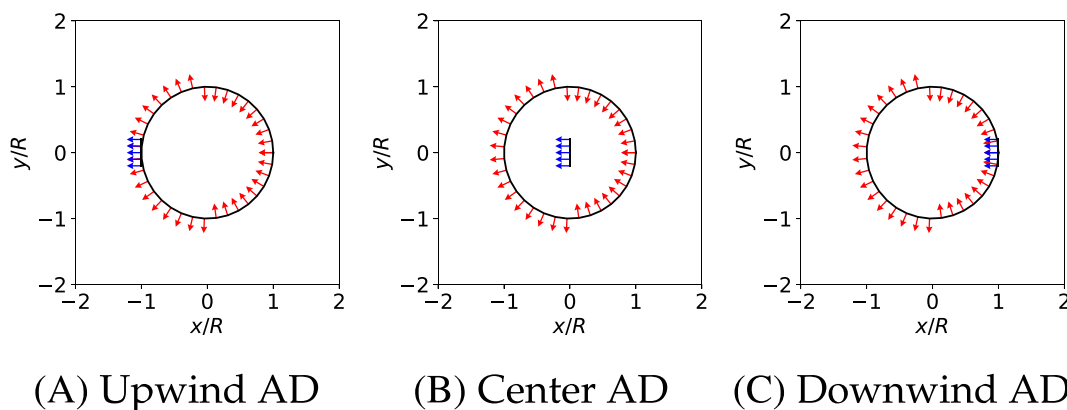


**FIGURE 10** (A–C) Force distribution for an idealized hybrid VAWT with a turbine-mode AD (force of AD is opposite to the inflow direction,  $c_{TAD} > 0$ ). AD, actuator disk; VAWT, vertical axis wind turbine.

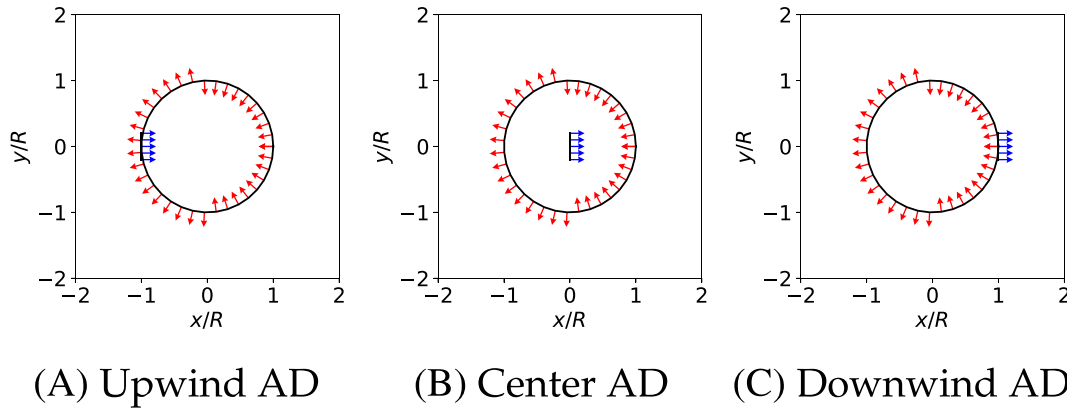


**FIGURE 11** (A–C) Force distribution for an idealized hybrid VAWT with a propeller-mode AD (force of AD is directed to the inflow direction,  $c_{TAD} < 0$ ). AD, actuator disk; VAWT, vertical axis wind turbine.

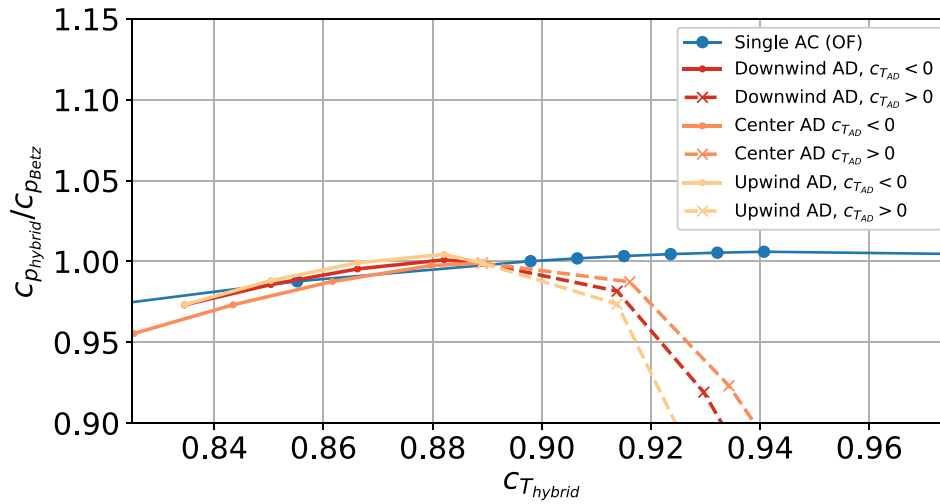


**FIGURE 12** Power coefficient of an idealized hybrid VAWT  $c_{p_{\text{hybrid}}}/c_{p_{\text{Betz}}}$  with varied  $c_{TAD}$ ,  $c_{TAC} = 0.89$ . VAWT, vertical axis wind turbine.

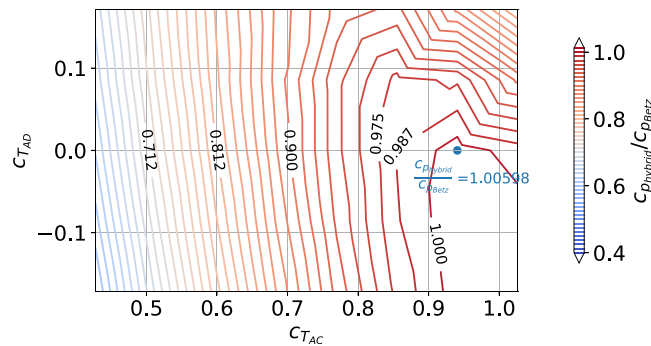


**FIGURE 13** Power coefficient of an idealized hybrid VAWT  $c_{p_{\text{hybrid}}}/c_{p_{\text{Betz}}}$  with downwind AD for different combinations of  $c_{TAD}$  and  $c_{TAC}$ . AD, actuator disk; VAWT, vertical axis wind turbine.

The contour of the power coefficient for different combinations of  $c_{TAD}$  and  $c_{TAC}$  is illustrated in Figure 13. The power coefficient between the idealized hybrid VAWT and single AC with the optimal thrust coefficient  $c_{T_{\text{Betz}}}$  is compared. It is observed that  $c_{p_{\text{hybrid}}}/c_{p_{\text{Betz}}}$  exceeds one at the right bottom of the figure where the inner disk operates as a propeller and the outer cylinder operates at near-optimal conditions. So, the power

coefficient of the idealized hybrid VAWT exceeds  $c_{p_{Betz}}$  when the inner AD operates in a propeller mode. The blue point is the power coefficient of the optimal single AC, showing the overestimation of our numerical model. This contour suggests that the propeller mode of the AD force contributes to the power compensation in the idealized hybrid VAWT configuration.

To determine the reason behind the power increase for the idealized hybrid VAWT with AD in a propeller mode, the power coefficient of the idealized hybrid VAWT with turbine-mode/propeller-mode downwind AD and their velocity field are studied. The difference between the non-dimensional axial velocity of an idealized hybrid VAWT with a downwind AD and the single AC  $\Delta U_x$  in the flow field is depicted in Figure 14. This is to explore the effect of force distribution on flow fields of the idealized hybrid VAWT. In the case of an idealized hybrid VAWT with a turbine-mode AD shown in Figure 14B, the high-energy conversion on the upwind side of the rotor leads to a deficit in kinetic energy, reducing the energy extraction on the downwind side. However, when the AD operates in a propeller mode, as shown in Figure 14A, it helps to mitigate the rotor blockage caused by this kinetic energy deficit and to generate a slighter wake expansion downstream.

As claimed in Sections 2.1 and 2.2, the vorticity-development depends on the force distribution of the actuator. The total force of the outer cylinder and inner disk (Figure 2c) is consistent with the force of a single disk (Figure 3). This indicates that adjusting the force distribution of AC would be the alternative to moving the inner AD. Similar studies have been conducted by Huang et al.,<sup>28</sup> where the force distribution was changed by pitch control of blades. In Section 3.2.2, we will further study the effect of force distribution on the power output of the idealized hybrid VAWT.

To further comprehend the operational conditions of the idealized hybrid VAWT, its power performance with specific  $c_{T_{AC}}$  and  $c_{T_{AD}}$  is compared with the corresponding theoretical AC with the same  $c_{T_{AC}}$ . The power performance of the hybrid VAWT with center AD is taken as an example to compare with the single AC with the same  $c_{T_{AC}}$  (Figure 12). The results of the power coefficient for the idealized hybrid VAWT are shown in Figure 15. The legend  $c_{p_{hybrid}}/c_{p_{AC,theoretical}}$  represents the ratio of the power coefficient of the idealized hybrid VAWT with specific  $c_{T_{AC}}$  over that of the single theoretical AC with the same  $c_{T_{AC}}$ . The results on the top-right of the figure are not presented due to the numerical instabilities of the high-thrust cases. Besides, the flow reversal behind actuators leads to significant unsteadiness in the predicted power. When a turbine-mode AD ( $c_{T_{AD}} > 0$ ) is employed, the value of  $c_{T_{AC}}$  should be lower to maintain or even increase  $c_p$  of the idealized hybrid VAWT compared with  $c_p$  of the AC with the same  $c_{T_{AC}}$ . On the other hand, when a propeller-mode AD ( $c_{T_{AD}} < 0$ ) is employed, the AC is expected to operate with a high  $c_T$  to maintain the same amount of  $c_p$ , thus compensating for the power consumption of propeller-mode AD. This analysis highlights the importance of selecting the appropriate operating mode and adjusting the thrust coefficients for the actuators in the idealized hybrid VAWT to optimize its power performance.

The optimal operational points for the idealized hybrid VAWT are analyzed based on predefined force conditions. When a specific  $c_{T_{AC}}$  is given, there is an optimal operational point for the inner disk to obtain the maximum  $c_p$  of the idealized hybrid VAWT. These optimal points, obtained from both numerical and theoretical solutions, are plotted in Figure 15. The results show that the optimal configurations of the idealized hybrid VAWT with a known  $c_{T_{AC}}$  occur when  $c_{T_{AC}} + c_{T_{AD}}$  is equal to 0.89. The theoretical results agree well with the numerical results.

To give further information for the design of the idealized hybrid VAWT, the operational conditions are compared under different given forces. The relation between  $c_{p_{hybrid}}/c_{p_{Betz}}$  and  $c_{T_{AD}}$  for an idealized hybrid VAWT with the center AD is shown in Figure 16. For given high-thrust cases  $c_{T_{AC}} \geq 0.85$ , the power coefficient of the idealized hybrid VAWT decreases with the increasing  $c_{T_{AD}}$ . While for low-thrust cases where  $c_{T_{AC}} \leq 0.76$ , the idealized hybrid VAWT exhibits a slight power increase when  $c_{T_{AD}}$  reaches a certain value. So, given a low  $c_{T_{AC}} \leq 0.76$  for the idealized hybrid VAWT, we should increase the thrust coefficient of the inner AD to get the maximum power. But given a high  $c_{T_{AC}} \geq 0.85$ , the power performance of the idealized hybrid VAWT will only be worse with the presence of the inner AD.

The relation between  $c_{p_{hybrid}}/c_{p_{Betz}}$  and  $c_{T_{AC}}$  for an idealized hybrid VAWT with the center AD is shown in Figure 17. The case of  $c_{T_{AD}} = 0.00$  represents the power coefficient of the single AC. It can be observed that the maximum power coefficient of the idealized hybrid VAWT

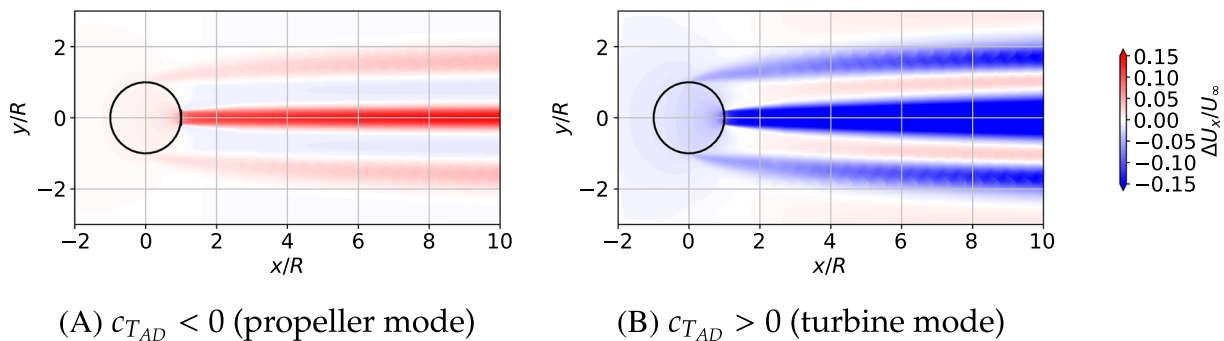


**FIGURE 14** (A, B) Difference of nondimensional axial velocity field between an idealized hybrid VAWT with downwind AD and the single AC,  $c_{T_{AC}} = 0.93$ ,  $c_{T_{AD}} = \pm 0.1$ .

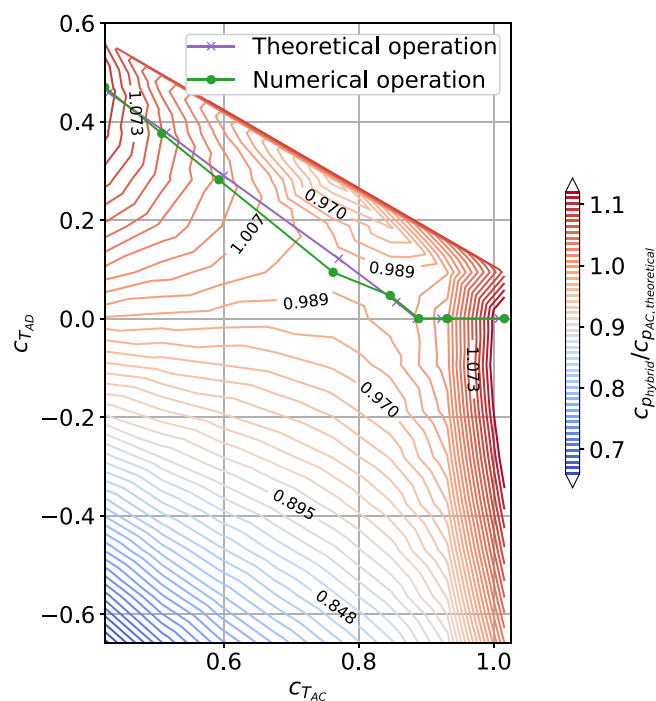


**FIGURE 15** Power coefficient of an idealized hybrid VAWT with center AD  $c_{p_{hybrid}}/c_{p_{AC,theoretical}}$  for different combinations of  $c_{T_{AD}}$  and  $c_{T_{AC}}$ . VAWT, vertical axis wind turbine.

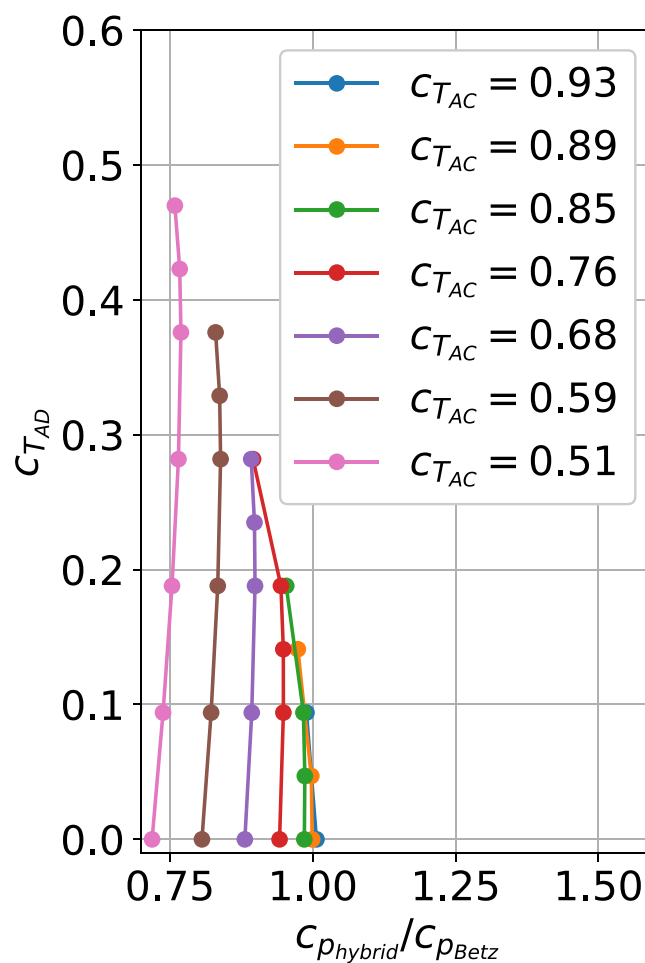


**FIGURE 16**  $c_{p_{hybrid}}/c_{p_{Betz}}$  versus  $C_{T_{AD}}$  for an idealized hybrid VAWT with center AD. AD, actuator disk; VAWT, vertical axis wind turbine.

decreases with the increasing  $c_{T_{AD}}$ . To achieve the power of the hybrid VAWT as  $c_{p_{hybrid}}/c_{p_{Betz}} = 0.7$ , the thrust of AC is supposed to increase with the decreasing given  $c_{T_{AD}}$ . In other words, given a low  $c_{T_{AD}}$  requires higher  $c_{T_{AC}}$  to gain the same amount of power as the given high  $c_{T_{AD}}$ .

### 3.2.2 | Adjusted force distribution on idealized Darrieus, representing AC

As analyzed in Section 3.2.1, the hybrid VAWT with a propeller-mode AD has a comparable power coefficient with a single Darrieus. It indicates that the propeller-mode AD effectively counteracts the nonoptimal force distribution of hybrid VAWT. Taking an example of an idealized hybrid VAWT with outer AC (representing the nonuniformly loaded Darrieus) and a center AD (representing the uniformly loaded Savonius),

the effect of the adjusted force distribution on the performance of the idealized hybrid VAWT is investigated. The angle  $\psi$  is proposed, referring to the range of adjusted force distribution for the outer AC. It is the angle between the x-axis and the starting point of the adjusted region on AC, as shown in Figure 18. In this study, the thrust coefficient of the inner AD is set as 0.1, and the outer AC has a nonuniform force distribution. The adjusted force distribution on the outer AC is nonuniform because of the superimposition of the force for propeller-mode AD and the force for AC operating at the optimal condition, shown in Figure 11A.

The power coefficients of a hybrid VAWT with and without adjusted force distribution on the outer AC are depicted in Figure 19.  $\psi = 0^\circ$  represents a hybrid VAWT with uniformly loaded AC and AD, shown in Figure 10B. And nonzero  $\psi$  represents a hybrid VAWT with adjusted force distribution on the outer AC, shown in Figure 18. The power coefficient of the hybrid VAWT is normalized by the numerical maximum power coefficient of the single AC  $c_{p_{opt}}$ . It is observed that the power coefficient increases and then decreases with the increase of angle  $\psi$ . The optimal

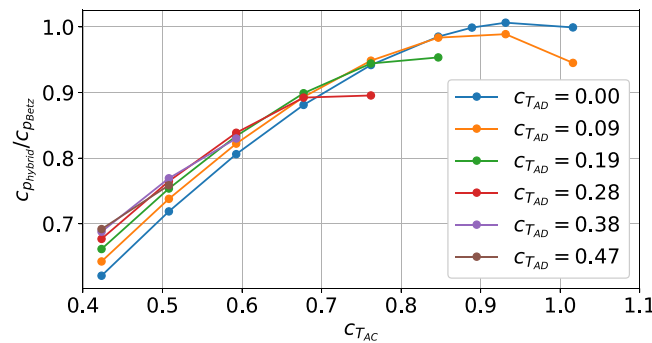


**FIGURE 17**  $c_{p_{hybrid}}/c_{p_{Betz}}$  vs  $c_{T_{AC}}$  for an idealized hybrid VAWT with center AD. AD, actuator disk; VAWT, vertical axis wind turbine.

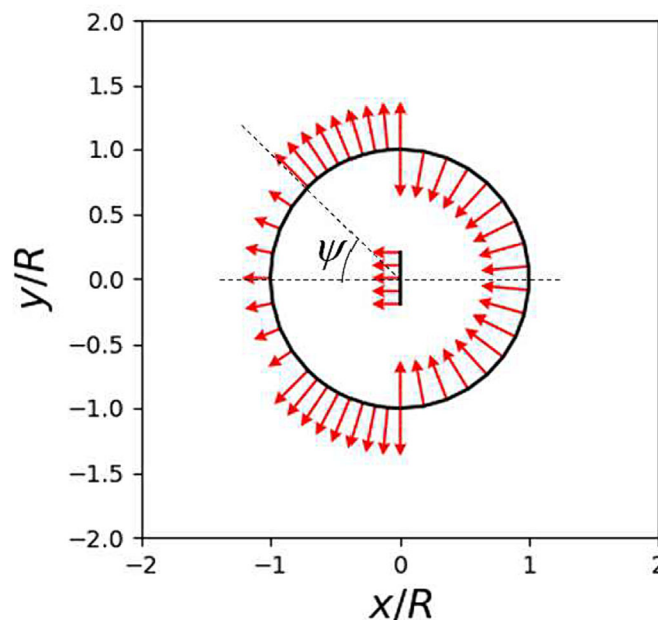


**FIGURE 18** A hybrid VAWT with adjusted force distribution. VAWT, vertical axis wind turbine.

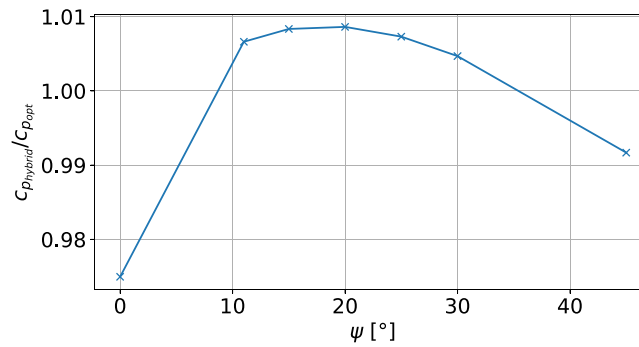


**FIGURE 19** Power coefficient  $c_p/c_{p_{opt}}$  of a hybrid VAWT with and without adjusted force distribution ( $c_{T_{AD}} = 0.1, c_{T_{adjusted}} = -0.1$ ). VAWT, vertical axis wind turbine.

$\psi$  is around  $20^\circ$ , in which case the power coefficient is 3.5% higher than the hybrid VAWT with uniformly loaded AC and AD. This indicates that power compensation occurs by adjusting force distribution in the outer AC. Among the studied cases of adjusted hybrid VAWT with varying  $\psi$ , angles ranging from  $8.25^\circ$  to  $34^\circ$  provide the optimal force distribution of the hybrid VAWT with no power losses. The adjusted force distribution in the upwind half of the AC leads to an optimal power output for the hybrid VAWT.

## 4 | CONCLUSIONS AND OUTLOOK

The flow mechanism of hybrid VAWT is complex due to the interaction between Darrieus and Savonius. It is known that the power output of the hybrid VAWT is reduced with the existence of the inner Savonius rotor. Many factors, such as airfoil efficiency and TSR, dominate the power output. Our understanding of power reduction is further improved by the research on the idealized turbine. To investigate the power performance of the idealized hybrid VAWT, the actuator disk and cylinder models are implemented in OpenFOAM. The following outcomes are concluded.

- The numerical actuator model is validated against the theoretical actuator model. The extracted maximum power from the numerical actuator cylinder model has a discrepancy of around 0.598% compared with  $c_{p_{Betz}}$ .
- The maximum power output of the idealized hybrid VAWT with a given  $c_{T_{AD}}$  is lower than that of a single actuator due to the nonoptimal force distribution on the hybrid case. This indicates that a significant power increase of a hybrid VAWT cannot be realized by varying geometrical and operational parameters. The hybrid configuration is only beneficial to the start-up performance instead of the power performance.
- Given one of the force distributions for the two actuators in an idealized hybrid VAWT, we can determine the optimal force distributions for the idealized hybrid VAWT. Given a low  $c_{T_{AC}} \leq 0.76$  for the idealized hybrid VAWT, we should increase the thrust coefficient of the inner AD to get the maximum power. While given a series of  $c_{T_{AD}}$  for the idealized hybrid VAWT, it requires a higher  $c_{T_{AC}}$  for low  $c_{T_{AD}}$  case to gain the same amount of power as the high  $c_{T_{AD}}$  case.
- The power loss in the idealized hybrid VAWT can be compensated by changing the force distributions of the inner AD, representing the idealized Savonius.  
The propeller-mode actuator balances off the power loss caused by the existence of the AD.
- Another form of power compensation is to adjust the force distribution of the outer AC. The power output of hybrid VAWT will be increased by adjusting the upwind force distribution of AC to compensate for power losses caused by the inner AD. Among the studied cases, the hybrid VAWT has an optimal force distribution when adjusting the force distribution at  $\psi = 8.25\text{--}34^\circ$ .

These findings contribute to a better understanding of the power performance of the hybrid VAWTs and suggest potential strategies for compensating for their power losses through control of force distribution.

It is important to acknowledge that the hybrid VAWT is unlikely to surpass the power output of a single Darrieus rotor by changing operational and geometrical conditions. Instead of striving for maximum power generation in this context, our attention should pivot toward more pragmatic approaches: enhancing the start-up performance of the hybrid VAWT while mitigating power losses and tuning the wind condition around the turbine (e.g., using wind deflectors).

The inherent design of the hybrid configuration introduces complexities that may restrict achieving power levels comparable with a single Darrieus design. The Savonius rotor, while aiding self-starting, can potentially lead to flow disturbances that impact overall power generation



efficiency. A study on blade-vortex interaction for a realistic hybrid VAWT is required to correlate the blade torque and vortex behavior. Furthermore, a concerted effort should be directed toward minimizing power losses associated with the interaction between the Darrieus and Savonius rotors. This also requires a deep understanding of blade-vortex interaction in the hybrid VAWT. Fine-tuning the design parameters and investigating control strategies can lead to a reduction in flow disruptions and wake interactions, ultimately translating into improved overall efficiency compared with a conventional hybrid VAWT.

While achieving higher power output remains a desirable goal, the hybrid VAWT's distinctive strengths lie in its capacity for self-starting and consistent performance across diverse wind conditions. Redirecting our focus toward optimizing these attributes can significantly enhance the practicality and relevance of hybrid VAWTs in the renewable energy landscape. By embracing this approach, we can pave the way for more effective utilization of wind energy resources and drive sustainable advancements in wind turbine technology.

## NOMENCLATURE

### ABBREVIATIONS

AC	Actuator cylinder
AD	Actuator disk
HAWT	Horizontal axis wind turbine
TSR	Tip speed ratio
VAWT	Vertical axis wind turbine

### GREEK SYMBOL

$\gamma$	Attachment angle
$\lambda$	Tip speed ratio
$\Omega$	Rotational speed
$\omega$	Vorticity
$\rho$	Flow density
$\theta$	Phase angle
$\nu$	Flow viscosity

### ROMAN SYMBOL

#### *a* INDUCTION FACTOR

$c_p$	Power coefficient, $\frac{P}{0.5\rho U_\infty^3 A}$
$c_T$	Thrust coefficient, $\frac{T}{0.5\rho U_\infty^2 A}$

$F$  Blade force

$P$  Turbine power output

$p$  Pressure

$Q_n$  Volume force in normal direction

$R_D$  Darrieus rotor radius

$R_S$  Savonius rotor radius

$R_{AC}$  Radius of actuator cylinder

$R_{AD}$  Radius of actuator disk

$R_{hybrid}$  Radius of hybrid VAWT

$T$  Thrust

$u$  Local velocity

$U_\infty$  Inflow velocity

$V$  Cell volume

$x$  Horizontal axis

$y$  Vertical axis

## ACKNOWLEDGEMENTS

Jingna Pan gratefully acknowledges financial support from China Scholarship Council: No. 201906450032.

## DATA AVAILABILITY STATEMENT

The data that support the findings of this study are available from the corresponding author upon reasonable request.

## ORCID

Jingna Pan  <https://orcid.org/0000-0001-5727-7105>

## REFERENCES

1. Fatahian H, Mohamed-Kassim Z, Chang WS. Insights into the flow dynamics and rotor performance of a Savonius turbine with dynamic venting using controllable flaps. *Phys Fluids*. 2022;34(12):127109.
2. Fatahian E, Ismail F, Ishak MHH, Chang WS. The role of wake splitter deflector on performance enhancement of Savonius wind turbine. *Phys Fluids*. 2022;34(9):95111.
3. Mat Yazik MH, Chang WS, Ishak MHH, Fatahian E, Ismail F. Effect of surface roughness and blade material on the performance of a stationary Savonius wind turbine under different operating conditions. *Phys Fluids*. 2023;35(3):35133.
4. Jain S, Saha UK. The state-of-the-art technology of h-type Darrieus wind turbine rotors. *J Energy Resour Technol*. 2020;142:1-25.
5. Castelli MR, Englaro A, Benini E. The Darrieus wind turbine: proposal for a new performance prediction model based on CFD. *Energy*. 2011;36(8):4919-4934.
6. Rezaeiha A, Kalkman I, Blocken B. Effect of pitch angle on power performance and aerodynamics of a vertical axis wind turbine. *Appl energy*. 2017;197:132-150.
7. Rezaeiha A, Montazeri H, Blocken B. Characterization of aerodynamic performance of vertical axis wind turbines: impact of operational parameters. *Energy Conv Manag*. 2018;169:45-77.
8. Sun X, Chen Y, Cao Y, Wu G, Zheng Z, Huang D. Research on the aerodynamic characteristics of a lift drag hybrid vertical axis wind turbine. *Adv Mech Eng*. 2016;8:1-11.
9. Pallotta A, Pietrogiamici D, Romano GP. Hybri—a combined Savonius-Darrieus wind turbine: performances and flow fields. *Energy*. 2020;191:116433.
10. Liang X, Fu S, Ou B, Wu C, Chao CYH, Pi K. A computational study of the effects of the radius ratio and attachment angle on the performance of a Darrieus-Savonius combined wind turbine. *Renew Energy*. 2017;113:329-334.
11. Chegini S, Asadbeigi M, Ghafoorian F, Mehrpooya M. An investigation into the self-starting of Darrieus-Savonius hybrid wind turbine and performance enhancement through innovative deflectors: a CFD approach. *Ocean Eng*. 2023;287:115910.
12. Pouransari Z, Behzad M. Numerical investigation of the aerodynamic performance of a hybrid Darrieus-Savonius wind turbine. *Wind Eng*. 2024;48(1):3-14.
13. Irawan EN, Sitompul S, Yamashita K-I, Fujita G. Computational fluid dynamics analysis on the improvement of hybrid Savonius-Darrieus NREL s809 at various fluid flows. In: 2023 4th International Conference on High Voltage Engineering and Power Systems (ICHVEPS); 2023:389-394.
14. Madsen HA. The Voith-Schneider wind turbine—some theoretical and experimental results. *Ph.D. Thesis*: Technical University of Denmark; 1980.
15. Ferreira CJS. The near wake of the VAWT: 2D and 3D views of the VAWT aerodynamics; 2009.
16. Jin G, Zou L, Jiang Y, Zong Z, Sun Z. A circle theorem technique to handle 2-D flows around arbitrary cylinders in discrete vortex method. *J Wind Eng Industr Aerodyn*. 2021;209:104496.
17. Pan J, Ferreira C, vanZuijlen A. Estimation of power performances and flow characteristics for a Savonius rotor by vortex particle method. *Wind Energy*. 2023;26(1):76-97. <https://doi.org/10.1002/we.2788>
18. Mohammed AA, Ouakad HM, Sahin AZ, Bahaidarah HMS. Vertical axis wind turbine aerodynamics: summary and review of momentum models. *J Energy Resour Technol*. 2019;141(5):50801. <https://doi.org/10.1115/1.4042643>
19. Froude RE. On the part played in propulsion by differences of fluid pressure. *Trans Instit Naval Archit*. 1889;30:390.
20. Madsen HA. The actuator cylinder—a flow model for vertical axis wind turbines. *Ph.D. Thesis*: Technical University of Denmark; 1982.
21. Madsen HA. On the ideal and real energy conversion in a straight bladed vertical axis wind turbine. *Ph.D. Thesis*: Technical University of Denmark; 1983.
22. Betz A. *Introduction to the theory of flow machines*: Pergamon Press; 1966.
23. OpenFOAM. Openfoam user guide. <https://www.openfoam.com/documentation/user-guide>; 2017.
24. Abdulkadirov R, Lyakhov P. Estimates of mild solutions of Navier-Stokes equations in weak Herz-type Besov-Morrey spaces. *Mathematics*. 2022;10:680.
25. De Tavernier D. Aerodynamic advances in vertical-axis wind turbines. *Ph.D. Thesis*: TU Delft; 2021.
26. Bouzaher MT, Hadid M. Active control of the vertical axis wind turbine by the association of flapping wings to their blades. *Proc Comput Sci*. 2015;52:714-722.
27. Pan J, Ferreira C, van Zuijlen A. A numerical study on the blade-vortex interaction of a two-dimensional Darrieus-Savonius combined vertical axis wind turbine. *Phys Fluids*. 2023;35(12):125152.
28. Huang M, Sciacchitano A, Ferreira C. On the wake deflection of vertical axis wind turbines by pitched blades. *Wind Energy*. 2023;26(4):365-387.

**How to cite this article:** Pan J, Ferreira C, van Zuijlen A. Performance analysis of an idealized Darrieus-Savonius combined vertical axis wind turbine. *Wind Energy*. 2024;1-16. doi:[10.1002/we.2904](https://doi.org/10.1002/we.2904)